# Synergistic effect of quercitin and pH-responsive DEAE-chitosan carriers as drug delivery system for breast cancer treatment

**Rafael de Oliveira Pedro[1], Francisco M Goycoolea[2], Susana Pereira[2], Carla C. Schmitt[1], Miguel G. Neumann[1*]**

[1]Instituto de Química de São Carlos, Universidade de São Paulo, Caixa Postal 780, 13560-970 São Carlos SP, Brazil

[2]Institute of Plant Biology and Biotechnology (IBBP), Westfälische Wilhelms-Universität Münster, Schlossgarten 3, Münster 48149, Germany.

oliveira.ibilce@hotmail.com

carla@iqsc.usp.br

*neumann@iqsc.usp.br
Tel. xx55-16-3373-9940
Fax xx55-16-3373-9941

## 1. Introduction

Drug carriers have been increasingly used to enhance the therapeutic effect of drugs by improving the pharmacokinetics and reducing its toxicity (BRIGGER; DUBERNET; COUVREUR, 2002; NEL et al., 2006; PEREZ-HERRERO; FERNANDEZ-MEDARDE, 2015). These systems may also regulate the drug release rate, while maintaining the biological concentration within an appropriate range. The development of the carriers can also include a strategy to increase the selectivity of the drug release towards cancer cells or tissues.

The ability of carriers to change its structure when stimulated by various physiological conditions can be exploited to start and control the release of drugs. Stimuli-responsive carriers can be developed to respond selectively to physiological changes such as temperature, ionic strength and pH. It has been shown that the high lactic acid production by cancer cells decrease the pH of tumour tissues due to the accumulation of $H^+$ ions (DAMAGHI; WOJTKOWIAK; GILLIES, 2013; VAUPEL; KALLINOWSKI; OKUNIEFF, 1989). Therefore, biopolymers like chitosan, that exhibits pH-sensibility due to the free amino groups present in its structure, might be apropriated compounds to carry drugs towards these cells. This polymer is composed by 2-amino-2-deoxy-D-glucopyranose and 2-acetamide-2-deoxy- D-glucopyranose units linked by glycosidic $\beta(1 \rightarrow 4)$ bonds.

The amino groups of chitosan can also be used as sites to chemically change the polymer backbone by introduction of groups of interest. Amphiphilic modifications of chitosan can be carried out to enhance the amphiphilic characteristics of the polymer, allowing it to self-assemble in aqueous solution. The nanoparticles or nanoaggregates formed by this method normally have a core-shell structure with a hydrophobic nucleus. Thus, it is possible to entrap hydrophobic molecules into the nanoaggregates. Chitosan is considered biocompatible, non-toxic and biodegradable (KEAN; THANOU, 2010; KUMAR, 2000; WANG et al., 2011), therefore suitable for biological applications. Therefore, chitosan-based systems can be used as pH-responsive carrier for hydrophobic drugs.

In this study, as pH-responsive amphiphilic chitosan was prepared by chemical derivatization of the primary amine present in D-glucosamine units using 2-chloro-N,N-diethylethylamine hydrochloride and dodecyl aldehyde as reagents. The behaviour, size, zeta potential and morphology of the self-assembled aggregates were investigated. A mathematical model was used to predict the diffusion type from the release profiles of quercetin, a model drug entrapped in the aggregates. The in vitro toxicity of the blank and loaded nanoaggregates

against breast cancer cell (MCF-7) were also evaluated. The biological assessments involved the hemocompatibility studies of the derivatives.

## 2. Experimental section

### 2.1. Materials

Chitosan powder (low molecular weight, deacetylation degree (DD) ≥ 85%), 2-chloro-N,N-diethylethylamine hydrochloride (DEAE), dodecyl aldehyde (DDA), acetic acid, sodium acetate, sodium hydroxide, and pyrene were reagent grade and used as received from Sigma Aldrich Chemical Co., Brazil. 3-(4,5-dimethylthiazol-2-yl)-2,5-diphenyltetrazolium bromide (MTT), RPMI-1640 cell culture medium and Pur-A-Lyzer™ Mini Dialysis Kit (MWCO 6-8 kDa) were purchased from Sigma-Aldrich GmbH, Germany. Ultrapure MilliQ water was used throughout.

### 2.2 Deacetylation of Chitosan

Deacetylated chitosan (D-CS), prepared by the deacetylation process described earlier (DE OLIVEIRA PEDRO; SCHMITT; NEUMANN, 2016), was used as starting material. The sample was characterized by $^{1}$H NMR, ATR-FTIR and viscosimetry.

### 2.3 Depolymerization of Chitosan

The molecular weight of chitosan was reduced by the depolymerisation process using oxidation with sodium nitrate in acid solution as described by TOMMERAAS et al. (2001). Briefly, 10.0 grams of previously deacetylated chitosan (D-CS) were solubilized in 555 ml of acetic acid solution (2 wt%) overnight, purged with nitrogen for 1 h under constant stirring and cooled at 4 °C. The stirring was suspended and 18.6 ml of aqueous sodium nitrite (231 mg) were added to the mixture. The reaction was kept in the absence of light at 4 °C for 18 hours. Afterwards, the resulting solution was precipitated with sodium hydroxide, centrifuged at 10,000 rpm, washed with deionized water and the obtained product (L-CS) was lyophilized. The average molecular weight of the polymer was characterized by viscosimetry.

## 2.4. Syntheses

### 2.4.1. DEAE-modified chitosan

The hydrophilic chitosan grafted with 2-chloro-N,N-diethylethylamine hydrochloride (DEAE) was prepared using low molecular weight chitosan (L-CS). 3.0 g of chitosan were dispersed in 338.1 ml of hydrochloric acid solution (0.1 M). Then, 3.5 g of DEAE was added and the pH of the solution was adjusted to 8.0 by addition of sodium hydroxide (2 M). The reaction was kept at pH approximately 8.0, under stirring and reflux for 2 hours at 65 °C. Afterwards, the solution was dialyzed (MWCO 12 kDa), first against water for 24 hours, then against sodium hydroxide solution (0.05 M) for another 24 hours and finally against deionized water for three days. The final product was then recovered by lyophilization and characterized by $^{1}$H NMR and ATR-FTIR.

### 2.4.2 Amphiphilic chitosans

A previously described method (DE OLIVEIRA PEDRO; SCHMITT; NEUMANN, 2016) was used to obtain the amphiphilic chitosan samples. Briefly, 3 g of DEAE-modified chitosan was dissolved in acetic acid (0.2 M, 330 mL) overnight and added drop-wise to 240 mL of ethanol. Dodecyl aldehyde (DDA) dissolved in ethanol (10 mL) was added and the mixture was stirred for 1 h at room temperature. Afterwards, sodium cyanoborohydride was added and the reaction continued for 24 h under stirring at room temperature. After dialysis (MWCO 12 kDa) against water for 3 days, the product was lyophilized and characterized by $^{1}$H NMR and ATR-FTIR.

## 2.5 Characterization techniques

A digital rolling-ball viscometer (Lovis 2000 MME, Anton Paar, Graz, Austria) was used to obtain the intrinsic viscosities of chitosan samples. Measurements were carried out at concentrations in the 3.0 – 7.0×10$^{-3}$ g/ml range at pH 4.5 using acetic acid (0.3 M)/sodium acetate (0.2 M) buffer. The average viscosimetric molecular weights of commercial chitosan (C-CS), deacetylated chitosan (D-CS) and depolymerized low molecular weight chitosan (L-CS) were determined from the intrinsic viscosities, $\eta$, using the Mark–Houwink equation and

the constants, a = 0.76 and K = 0.076 mL/g for C-CS and, a = 0.82 and K = 0.076 mL/g for D-CS and L-CS, as suggested by RINAUDO; MILAS; LEDUNG (1993).

$^{1}$H NMR spectra were recorded on an Agilent 400/54 Premium Shielded spectrometer at 70 °C after 10 mg of chitosan samples were completely solubilized in 1 mL of deuterium oxide ($D_2O$) and 10 μL of deuterium chloride.

Attenuated total reflectance Fourier transform infrared spectroscopy (ATR-FTIR) analysis (Perkin Elmer Frontier™ FTIR spectrometer, Perkin Elmer, USA) was performed on freeze-dried samples to confirm the occurrence of the reaction between chitosan and DEAE and DDA. All spectra were recorded at room temperature and 4 scans were averaged over the of 4000–600 $cm^{-1}$ range.

Critical aggregation concentration (CAC) of polymeric self-assembling aggregates was measured by fluorescence spectrophotometry (Hitachi F4500 spectrophotometer) using pyrene as the fluorescence probe. 2 mL of buffer (acetic acid/sodium acetate or phosphate-buffered saline) was added to a quartz cuvette with 1 μL of a stock solution of pyrene (1 mM) in methanol. Afterwards, 10 μL of concentrated stock solutions of the derivatives samples (2.0 g/L) were added to buffered aqueous solutions of pyrene ($5.0\times10^{-6}$ M) under magnetic stirring, and fluorescence spectra were recorded after each addition. Pyrene was excited at 310 nm and its emission spectra were recorded from 350 to 500 nm. The CAC values were estimated from the plot of the intensity ratio between the first (373 nm) and the third (382 nm) vibronic peaks of pyrene spectra versus log C (concentration in g/L).

## 2.6 Particle size distribution, zeta potential and morphology of the nanoaggregates

The size distribution of the aggregates were determined at 0.1g/L concentration and pH 5.0 (acetate buffer) and 7.4 (phosphate buffer) using dynamic light scattering with non-invasive back scattering (DLS-NIBS) at an angle of 90º. The ζ-potential was measured by mixed laser Doppler velocimetry and phase analysis light scattering (M3–PALS). A Malvern Zetasizer NanoZS (Malvern Instruments Ltd., Worcestershire, UK) fitted with a red laser (λ = 632.8 nm) at 25 °C was used to perform both determinations.

The morphological characteristic of the nanoaggregates were observed using a JEM2100 LaB6 (Jeol, Japan) Transmission Electron Microscope operating at 200 keV. 20 μL of the

prepared sample solution was dropped onto the carbon-coated 200 mesh copper grid. The grids were air dried for 20 min and post-stained with phosphotungstic acid at 2%.

## 2.7 Drug loading and in vitro release

The hydrophobic drug quercetin (QCT) was loaded into the cores of the DEAE-CS nanoaggregates. 20 mg of the polymers were dispersed in 3 ml of buffer solution (pH = 5.0 or pH = 7.4) under continuous stirring for 8 hours. Afterwards, the drug previously solubilized in ethanol was added to the nanoaggregate solutions and the mixture was allowed to stir for 4 h. Then, the loaded nanoaggregates were isolated by centrifugation at 15,000 rpm for 50 min at 15º C. A proper calibration curve was used to determine the free QCT concentration in the supernatant using UV-visible spectrophotometry. The entrapment efficiency (EE) and the drug loading efficiency (DL) were calculated from the following equations :

$$EE(\%) = \frac{(total\ drug\ weight - free\ drug\ weight\ )}{(total\ drug\ weight)} x100\% \quad (1)$$

$$DL(\%) = \frac{(total\ drug\ weight - free\ drug\ weight)}{(loaded\ drug\ weight + nanoagreggates\ weight)} x100\% \quad (2)$$

The in vitro drug release tests were carried out by dispersing the nanoparticles loaded into buffer solution (pH = 5.0 and pH = 7.4). Subsequently, this solution was transferred to a Pur-A-Lyzer™ Mini Dialysis Kit (MWCO 6-8 kDa) and immersed in 35 mL of release medium (respective buffer solutions), maintained under gentle stirring at 37 °C. At predetermined intervals, 3 mL aliquots were taken of release medium and replaced by the same volume of buffer solution. The concentration of the released drug was determined by UV-visible spectrophotometry (NABID et al., 2011). The Korsmeyer–Peppas model (Eq. (3)) was used to determine drug release mechanism from nanoaggregates (COSTA; MANUEL; LOBO, 2001; KORSMEYER et al., 1983):

$$\frac{M_t}{M_\infty} = kt^n \quad (3)$$

Where $M_t$ is the mass of QCT released at time t, $M_\infty$ represents the total mass of QCT to be released and k is a constant that depends on the structural characteristics of the

nanoaggregates and the solvent/material interactions. The exponent n indicates the type of diffusion. The diffusion will be Fickian when n = 0.43 and will involve Case II transport when n = 0.85. Anomalous diffusion occurs when n is between these values, and when n > 0.85 the diffusion involves super-Case II transport. For polydispersed systems based in spherical particles a value for n lower than 0.43 is possible and is also considered Fickian (RITGER; PEPPAS, 1987). The portion of the release curve where $M_t/M_\infty < 0.6$ was used for the determination of the n exponent.

## 2.8 In vitro cytotoxicity assay

The cytotoxicity of the free drug, blank and loaded nanoaggregates was evaluated by MTT assay. Briefly, 100 µl of MCF-7 cell suspension was transferred to a 96-well tissue culture plate (~$10^4$ cells per well or ~$10^5$ cells/ml) and allowed to attach for 24 h. After the cells were washed once with supplement-free medium, the sample was added and the cells were incubated for 24 h. Afterwards, the samples were removed, the wells were washed twice with supplement-free medium and replaced with 100 µl of medium. 25 µl of MTT solution in PBS (5 mg/ml) were added to each well. After 4 h of incubation the medium was removed and the dye was dissolved in DMSO. Orbital shaking at 300 rpm for 15 min was used to completely solubilize the crystals and the absorbance was measured at λ = 570 nm in a microplate reader (Safire, Tecan AG, Salzburg, Austria). Relative viability values were calculated by dividing individual viabilities by the mean of the negative control (untreated cells). 4% Triton X-100 in PBS was used as a positive control.

## 2.8 Blood compatibility tests

The hemocompatibility tests were carried out using freshly collected pig blood. 800 µl of blood were diluted with 1 ml of PBS buffer. 1 mg of nanoaggregates were then dispersed in 1 ml of PBS buffer and incubated at 37 °C for 30 minutes. After addition of 20 µl of diluted blood, the tubes were incubated for 60 minutes at 37 °C with gentle agitation. The absorbance of the samples was checked using a UV-Vis spectrometer at 545 nm and the hemolysis ratio (HR) was calculated by the following equation:

$$HR(\%) = \frac{A_{sample} - A_{PBS}}{A_{water} - A_{PBS}} x100\% \quad (4)$$

Where $A_{sample}$, $A_{PBS}$ and $A_{water}$ are the absorbance at 545 nm of blood samples treated with nanoaggregates, PBS (negative control) and water (positive control), respectively.

## 3. Results and discussion

### 3.1. Characterization of the amphiphilic derivatives

The commercial chitosan was deacetylated and depolymerized before further modifications in order to reduce its toxicity (PARK et al., 2011) and improve the self-assembling properties of the amphiphilic derivatives (RINAUDO, 2006). The molecular weight for commercial (C-CS), deacetylated (D-CS) and deacetylated with low molecular weight (L-CS) chitosans are shown in Table 1.

**Table 1.** Amphiphilic derivatives characterization and viscosity-average molecular weight.

| Sample | DD[a] (%) | $DS_1$[b] (%) | $DS_2$[c] (%) | Mv (kDa) |
|---|---|---|---|---|
| C-CS | 84.3 | - | - | 82.4 |
| D-CS | 97.1 | - | - | 50.4 |
| L-CS | 97.1 | - | - | 3.8 |
| L-CS-$DEAE_{40}$ | - | 38.5 | - | - |
| L-CS-$DEAE_{40}D_5$ | - | 38.5 | 5.1 | - |
| L-CS-$DEAE_{40}D_{28}$ | - | 38.5 | 28.0 | - |

[a] Deacetylation degree.
[b] Degree of substitution at the hydrophilic chain.
[c] Degree of substitution at the hydrophobic chain.

The tertiary amino group DEAE was added to the main chain of the chitosan by nucleophilic substitution of the C-2 amine groups. The L-CS sample was used as starting material and the derivatives were characterized by $^1$H NMR and FTIR. The degree of deacetylation (DD), determined from $^1$H NMR spectra, was obtained from the areas of the peaks at $\delta$ = 2.35 ppm (resonance of the acetamidomethyl protons) and at $\delta$ = 5.21 ppm (resonance of the anomeric proton doublet – H2) according to our previous report (DE OLIVEIRA PEDRO et al., 2013). The DD (expressed in $-NH_2$ mol%) was 84.2% for C-CS and 97.5% for D-CS and L-CS.

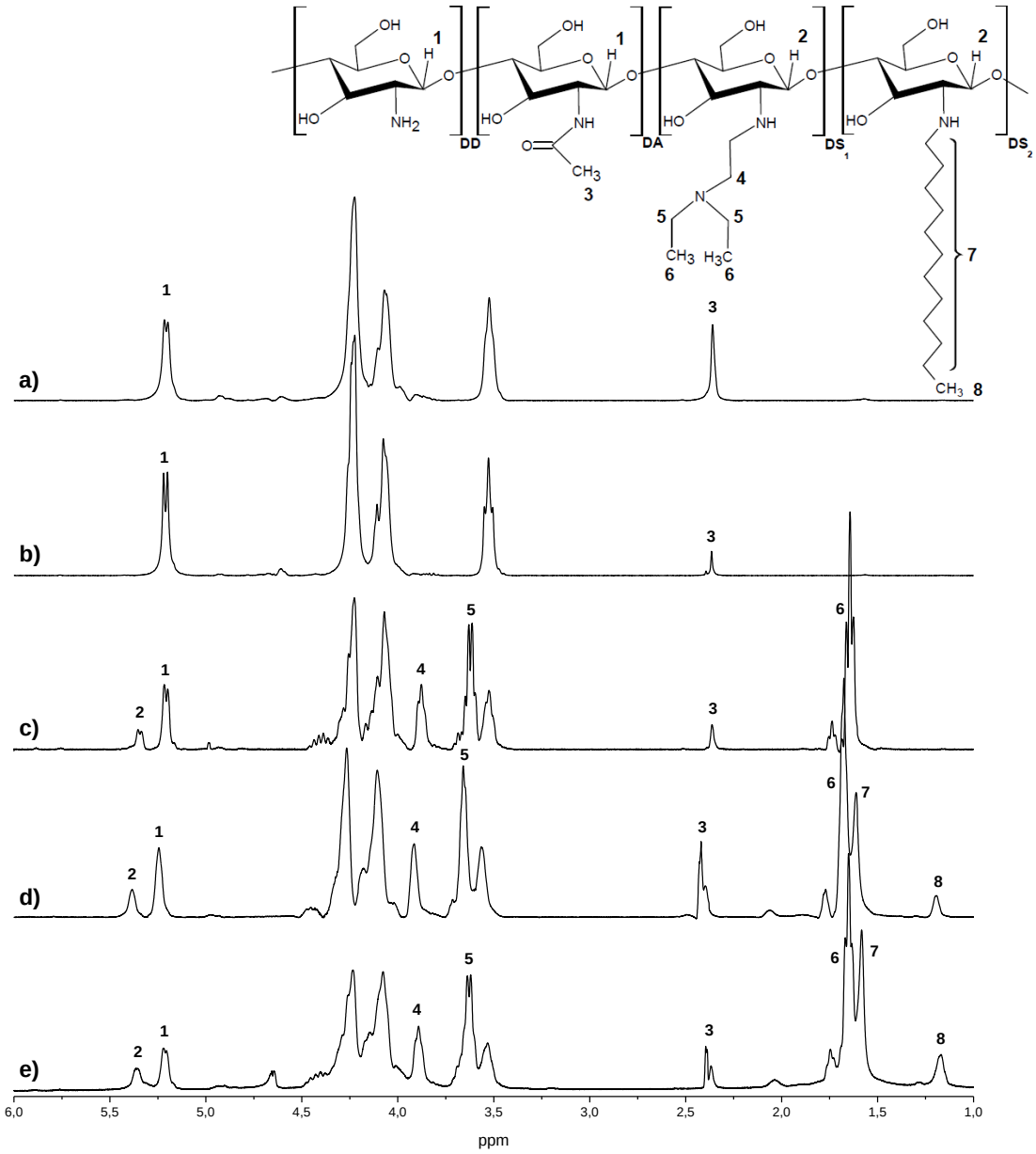


**Fig. 2.** $^{1}$HNMR spectra of a) commercial chitosan (C-CS), b) deacetylated low molecular weight chitosan (L-CS), c) the hydrophilic derivative containing 38.5% of DEAE (L-CS-DEAE$_{40}$), and its amphiphilic derivatives containing d) 38.5% of hydrophilic and 5.1% hydrophobic chain (L-CS-DEAE$_{40}$D5) and e) 38.5% of hydrophilic and 28.0% hydrophobic chain (L-CS-DEAE$_{40}$D$_{28}$).

Fig. 2c shows the $^{1}$H NMR spectrum of DEAE-chitosan derivative. The resonance of the methyl protons (NH-CH$_2$-C**H$_3$**) of the DEAE moieties can be attributed to the singlet at δ =

1.64 ppm. The signals at δ = 3.62 and 3.88 ppm correspond to the methylene protons of NH-$CH_2C\mathbf{H_2}N(CH_2CH_3)_2$ and NH-$CH_2CH_2N(C\mathbf{H_2}CH_3)_2$ , respectively. The degree of substitution by DEAE ($DS_1$) was determined from the areas at δ = 1.64 ppm and signals due to the anomeric protons of substituted (δ = 5.36 ppm) and unsubstituted (δ = 5.25 ppm) glucosamine residues. Using Eq. 5 the degree of substitution $DS_1$ of L-CS-$DEAE_{40}$ could be calculated as being 38.5%.

$$\overline{DS_1}(\%) = \left(\frac{I_{1.64}}{6.[I_{5.25}+I_{5.36}]}\right).100\% \quad (5)$$

The $^1$H NMR spectra for the amphiphilic derivatives are shown in Fig 2d and e. The signal at δ = 1.57 ppm is related to the resonance of the methylene hydrogens in the C12 chain of the DDA substituent. The resonance of the methyl group present in the C12 moieties shows signal at δ = 1.18 ppm. Eq. 6 was used to calculate the degree of substitution ($DS_2$) by the hydrophobic dodecyl group (DDA), comparing the signals at δ = 1.18 ppm with signals of the anomeric protons (δ = 5.36 ppm and δ = 5.25 ppm) (DE OLIVEIRA PEDRO; SCHMITT; NEUMANN, 2016).

$$DS_2(\%) = \left[\frac{I_{1.18}}{3(I_{5.25}+I_{5.36})}\right] \times 100\% \quad (6)$$

The $DS_2$ for L-CS-$DEAE_{40}D_5$ was 5.1% and for L-CS-$DEAE_{40}D_{28}$ was 28.0%. Table 1 shows the degrees of substitution (DS) at different sites of the compounds.

Fig. 3 shows the FTIR spectra for deacetylated low molecular weight chitosan (L-CS), DEAE-grafted chitosan derivative (L-CS-$DEAE_{40}$), and the amphiphilic derivatives L-CS-$DEAE_{40}D_5$ and L-CS-$DEAE_{40}D_{28}$. The broad band around 3400 $cm^{-1}$ is related to the axial stretching vibration of the hydroxyl groups (O–H) of chitosan chains and residual water aligned with the aliphatic C–H stretching band.

The peak intensity around 1595 $cm^{-1}$ is related to the N-H bending vibration of the primary amino group (MITRA et al., 2013). With the insertion of the DEAE and DDA groups in the chitosan backbone by nucleophilic substitution, the intensity of this peak decreases, supporting the evidence found by $^1$H NMR that the reactions occurred at the primary amine (–$NH_2$) of the chitosan chain.

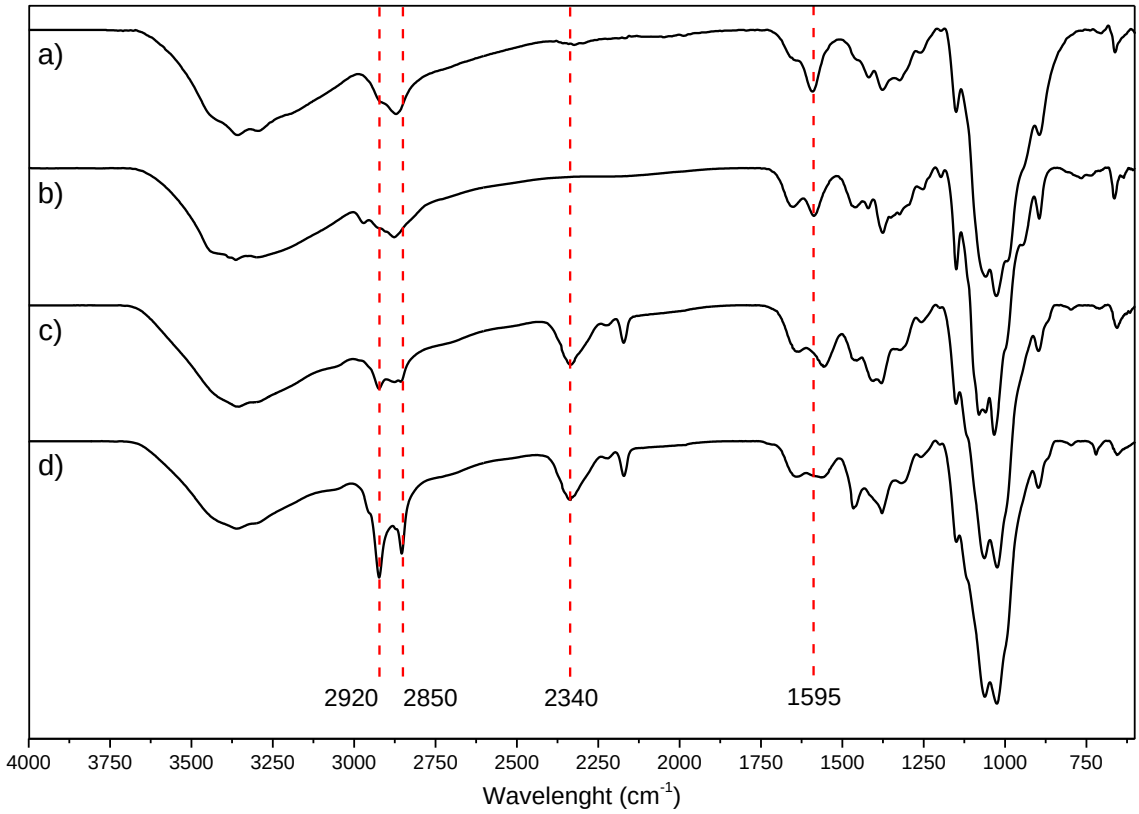


**Fig. 3.** FTIR spectra of (a) deacetylated low molecular weight chitosan (L-CS), (b) DEAE-grafted chitosan (L-CS-$DEAE_{40}$), and its amphiphilic derivatives (c) L-CS-$DEAE_{40}D_5$ and (d) L-CS-$DEAE_{40}D_{28}$.

The amphiphilic samples (Fig. 3c and d) exhibit characteristic peaks at 2920 and 2850 $cm^{-1}$ due to the axial deformation of the carbon-hydrogen bond of the $CH_3$ and $CH_2$ groups, respectively. Those signals become sharper with the increase of the DS by DDA (L-CS-$DEAE_{40}D_5$ vs. L-CS-$DEAE_{40}D_{28}$) which is in agreement with the DS quantified by $^1H$ NMR. The amphiphilic samples also show a typical peak at 2340 $cm^{-1}$ related to the vibration of the DDA-substituted amino groups (ROBLES et al., 2014).

## 3.2 Aggregation in aqueous solution

The amphiphilic modification of the chitosan reported here allows it to self-assembly to form nanoparticles or nanoaggregates. The self-assembly phenomena is driven by the orientation of hydrophilic groups towards the aqueous media, creating hydrophobic microdomains inside the structure, which allows the encapsulation of hydrophobic drugs by the aggregates. For a

better understanding of the aggregation behaviour of these samples in aqueous solution pyrene was used as fluorescence probe. The $I_1/I_3$ (373 nm/382 nm) ratio of the emission intensities is used to measure the presence of hydrophic microenvironments. It decreases slowly with the formation of nanoaggregates due to its displacement from hydrophilic to hydrophobic sites.

The dependence of the CAC with pH for both amphiphilic derivatives are shown in Table 2. At pH lower than the pKa (~6.2) of the residual free amine groups of the chitosan backbone, the polymer will be protonated increasing its hydrophilicity. Therefore, the onset of the aggregation occurs at lower concentrations at higher pH. The hydrophilicity of the derivatives is also affected by the DS of the hydrophobic DDA group. The aggregates forms more hydrophobic cores when the degree of substitution by C12 chain increases due to the stronger water repulsion among the chains, lowering the CAC.

**Table 2.** CAC of the amphiphilic derivatives at different pH

| | CAC ($g/L\times10^{-3}$) | | | |
|---|---|---|---|---|
| Sample | pH 4.0 | pH 5.0 | pH 6.2 | pH 7.4 |
| L-CS-DEAE$_{40}$D$_5$ | 5.0 | 3.7 | 3.2 | 2.7 |
| L-CS-DEAE$_{40}$D$_{28}$ | 3.9 | 3.5 | 2.6 | 1.5 |

3.3 Drug Loading and in vitro Release

The CAC determinations suggests that the samples can self-assemble in aggregates with hydrophobic cores, which allows them to encapsulate hydrophobic molecules. Quercetin, a widely used natural hydrophobic flavonoid, with many biological effects including a significant effect on the growth of numerous human and animal cancer cell lines (CHOU et al., 2010; LAROCCA et al., 1990; PRALHAD; RAJENDRAKUMAR, 2004), was used as drug model. Despite its many interesting properties, the use of QCT in the pharmacological field is restricted by its low aqueous solubility.

The entrapment efficiency and the drug loading for the amphiphilic samples are shown in Table 3. The EE slightly increased from 73 to 78 % with the DS of the DDA chain while the DL decreased from 5.2 to 4.3%. This behaviour can be explained by the higher number of hydrophobic moieties inside the core of the aggregates formed with higher DS of the C12 chain. These results are better to those reported in experiments involving similar systems reported in the literature (DU et al., 2015; WU et al., 2016; WU et al., 2014).

**Table 3.** Characteristics of the nanoaggregates

| Sample | Blank Nanoaggregates | | | Drug-Loaded Nanoaggregates | | | | |
|---|---|---|---|---|---|---|---|---|
| | Size (d.nm) | PDI | Zeta (mV) | Size (d.nm) | PDI | Zeta (mV) | EE (%) | DL (%) |
| L-CS-DEAE$_{40}$D$_{5}$ | 169 ± 14 | 0.678 ± 0.053 | 24.1 ± 1.1 | 410 ± 36 | 0.662 ± 0.021 | 40.1 ± 1.9 | 73 ± 3 | 5.2 ± 0.7 |
| L-CS-DEAE$_{40}$D$_{28}$ | 293 ± 25 | 0.402 ± 0.123 | 13.4 ± 3.1 | 405 ± 31 | 0.430 ± 0.016 | 41.7 ± 2.1 | 78 ± 3 | 4.3 ± 0.3 |

The in vitro release of QCT from drug-loaded nanoaggregates was performed by dispersing the nanoparticles in buffer solutions (pH = 5.0 and pH = 7.4). Fig. 4 shows that a burst release phenomenon occurred during the first 8 h of the in vitro release due to weakly attached QCT on the surface of the polymer (HUANG; BRAZEL, 2001). The burst release effect was slower for the L-CS-DEAE$_{40}$D$_{5}$ sample (Fig. 4a) at both pHs. After the first 8 h, QCT was steadily released from the nanoaggregates, achieving a cumulative release of approximately 50% after 96 h for both samples and pHs. The slow release rate observed may be ascribed to the strong interactions among the DDA chains and the hydrophobic drug. This behaviour may have also been due to low solubility of QCT in the release solution associated with a barrier that limited the access of the water inside the aggregates.

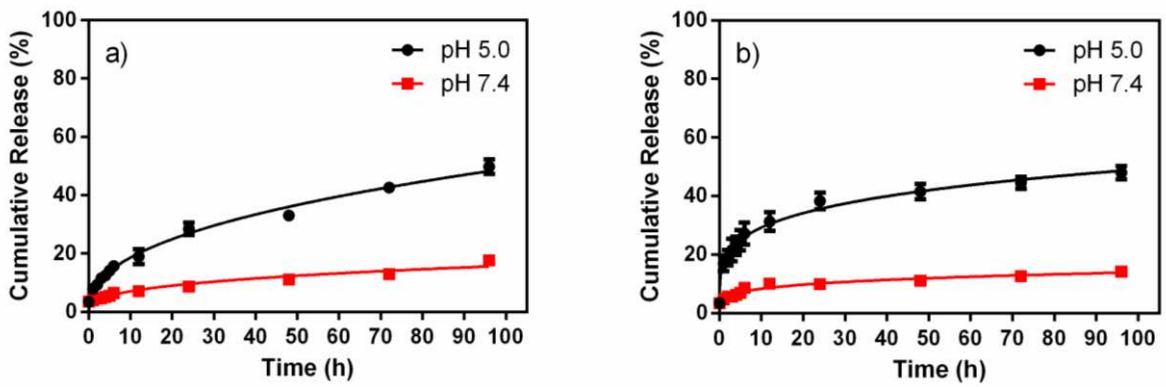


**Fig. 4.** In vitro release profile of QCT from a) L-CS-DEAE$_{40}$D$_{5}$ and b) L-CS-DEAE$_{40}$D$_{28}$ at pH 5.0 and 7.4 and 37 ºC.

pH also has a significant effect over the drug release. As shown in Fig. 4, both samples exhibit a much more prominent release at pH 5.0. This can be attributed to the protonation of the remaining free amino groups of the chitosan backbone that occurs at pH 5.0, leading to the formation of hydrogen bonds between water molecules and the protonated amino groups.

Consequently, the inner core of the nanoaggregates is less hydrophobic, therefore, the interactions with QCT is weaker and the release is facilitated. This regulation by the pH can be used to trigger the release at cancerous tissues due to the fact that the pH in these areas is acidic in opposite to physiological pH (7.4) (STUART et al., 2010; TANNOCK; ROTIN, 1989). Lactic acid produced as a by-product of anaerobic glucose metabolism lowers the pH of the cancer area. Additionally, acidic pH sites can also be found in endosomes and lysosomes, within cancer cells (AYDIN; PULAT, 2012). This pH-regulated behaviour of the DEAE-based amphiphilic samples reveals the pharmaceutical potential of this systems.

The Korsmeyer-Peppas release model was used to understand the release kinetics and mechanisms of QCT. This model was applied up to 60% of the final weight of the released drug. As shown in Table 4, the $R^2$ values for both sample at pH 5.0 were close to 1 and much lower at pH 7.4, due to the fact that the release rate at this pH is much lower. Furthermore, the poor fitting release data at pH 7.4 suggests that there is change in surface area as a function of pH and also may confirm that the change depends on the pH of the release environment. Therefore, the n exponent indicates that the Fickian diffusion is the controlling factor in drug release.

**Table 4:** Mathematical parameters of the release data.

| Sample | pH | k | n | Correlation value ( $R^2$) |
|---|---|---|---|---|
| L-CS-DEAE$_{40}$D$_5$ | 5.0 | 7.31 ± 1.16 | 0.41 ± 0.11 | 0.9768 |
| | 7.4 | 3.72 ± 1.26 | 0.26 ± 0.25 | 0.8935 |
| L-CS-DEAE$_{40}$D$_{28}$ | 5.0 | 16.24 ± 1.29 | 0.26 ± 0.05 | 0.9620 |
| | 7.4 | 4.99 ± 0.54 | 0.22 ± 0.03 | 0.8642 |

3.4 Size and morphology of the nanoaggregates

The particle size distribution, polydispersity indices (PDI) and zeta potential of the blank and loaded aggregates were evaluated by DLS measurements. As shown in Table 3, the average size increased from 169 to 263 nm with the higher hydrophobic DS for the blank nanoaggregates and was about the same for the loaded samples (410 and 405 nm). The PDI does not change significantly with the loading of the drug. It also suggests that the sample L-CS-DEAE$_{40}$D$_5$ has a narrower size distribution when compared to L-CS-DEAE$_{40}$D$_{28}$, although both samples are characterized by widely participation of extra associations among

the aggregates. The zeta potential reveals a positive charge at the surface of the nanoaggregates and increases for both samples after loading QCT, which suggests good stability under these conditions (HONARY; ZAHIR, 2013).

The morphology of the blank nanoaggregates were evaluated further by TEM. Fig 5c-d show that the aggregates exhibited spherical morphology and relative homogeneity with average size consistent with the DLS findings. The slightly differences in the diameter may be attributed to the fact that TEM analysis was carried out in dried particles, whereas DLS measurements were influenced by the interaction of the samples with water. No further agglomeration was observed.

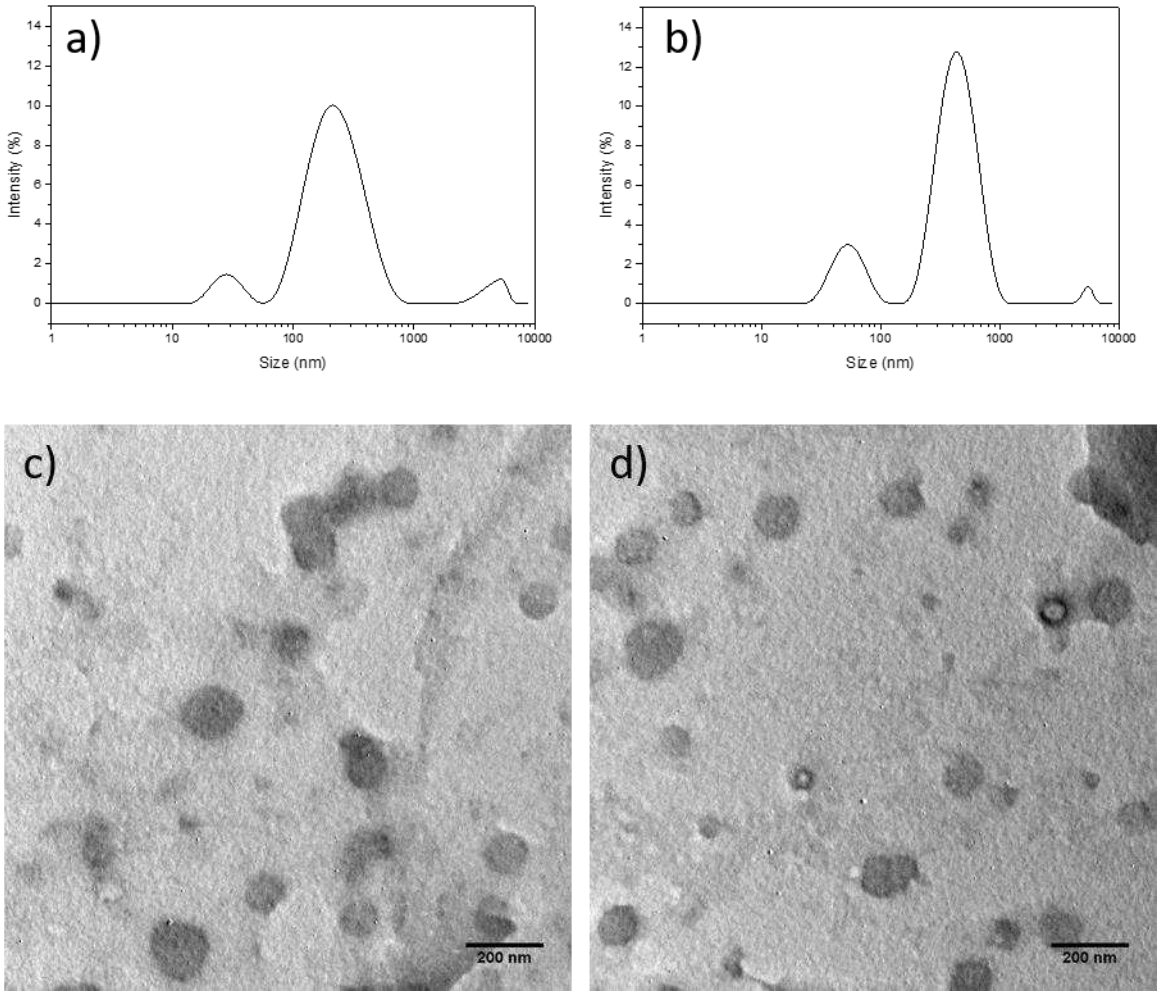


Fig. 5. Particle size distributions of a) L-CS-DEAE$_{40}$D$_{5}$ and b) L-CS-DEAE$_{40}$D$_{28}$ blank nanoaggregates. TEM images of blank nanoaggregates comprising c) L-CS-DEAE$_{40}$D$_{5}$ and d) L-CS-DEAE$_{40}$D$_{28}$ samples.

## 3.5 In Vitro Cytotoxicity Studies

The cell cytotoxicity of chitosan and its derivatives was carried out on breast cancer cell line MCF-7. The cells were grown in RPMI-1640 cell culture medium at 10% $CO_2$ and 37 ºC. The polymer concentrations used for the blank nanoaggregates refer to that used for the QCT-loaded samples.

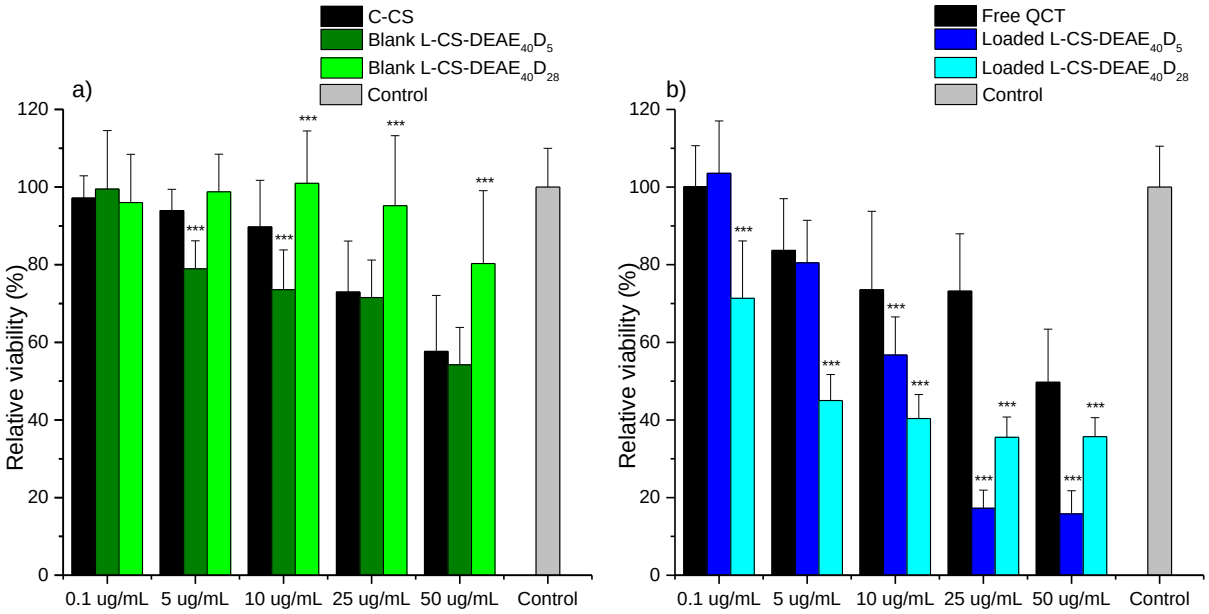


**Fig. 6.** Cytotoxicity of nanoaggregates against MCF-7 cells in 96-well plates determined using the MTT assay. (a) Relative cell viability following treatment with commercial chitosan (C-CS) and blank nanoaggregates at increasing concentrations. (b) Relative cell viability following treatment with free QCT and loaded nanoaggregates. Absolute concentrations refers to concentration of QCT. For all experiments, cells were incubated for 24 h. Mean values ± SD. (n = 3, *** $p < 0.001$).

Fig. 6a) indicates that the sample L-CS-$DEAE_{40}D_{28}$ has less cytotoxic effect when compared with C-CS or L-CS-$DEAE_{40}D_5$, having cell viability over 80% at the highest concentration. This result is in agreement with those by MERCHANT et al. (2014) using hydrophobically modified chitosan. Although the cytotoxicity of the sample L-CS-$DEAE_{40}D_5$ was larger than

that of chitosan at 5 and 10 µg/mL concentrations, at higher concentrations no significant statistic difference was observed. Nevertheless, the viability was larger than 50% for the samples at all concentrations, indicating adequate properties for biological application.

MCF-7 cells were also incubated with free QCT and loaded nanoaggregates. As shown in Fig 6b), the chitosan derivatives showed a significant reduction of viability of the breast cancer cells over the free QCT. The sample L-CS-DEAE$_{40}$D$_{28}$ was better than the free QCT even in the lowest concentration while the sample L-CS-DEAE$_{40}$D$_{5}$ showed very strong cell viability reduction at higher concentrations. The results clearly indicates that the amphiphilic chitosan derivatives can significantly improve the anticancer drug effect of QCT in vitro.

## 3.6 Blood compatibility tests

The in vitro erythrocyte-induced hemolysis is a reliable and extensively used test to estimate the blood compatibility of the new materials (LI et al., 2012;  RAO; SHARMA, 1997; ZHANG et al., 2008). A significant interaction with erythrocytes might influence the circulation of the nanoaggregates. The contact between the polymeric chains of chitosan with blood can lead to the rupture of the erythrocyte membrane and the release of hemoglobin. The hemolysis ratio for the sample L-CS-DEAE$_{40}$D$_{5}$ and L-CS-DEAE$_{40}$D$_{28}$ were 0.31 ± 0.01 and 0.50 ± 0.04, respectively. The results are far smaller than 5% of the international standard, suggesting that the samples have suitable hemocompatibility for biological applications.

## 4. Conclusions

Chitosan was chemically modified with 2-chloro-N,N-diethylethylamine hydrochloride and dodecyl aldehyde in order to obtain amphiphilic derivatives that can self-assemble in aqueous solution. Pyrene studies revealed that the aggregates with hydrophobic core were formed at concentrations over 0.015 g/L.

Drug loading experiments showed that the aggregates could efficiently entrap up to 78 % of the drug quercetin and that the pH has a significant role in the drug release process. The Korsmeyer-Peppas release model indicates that the Fickian diffusion is the controlling factor in drug release.

DLS experiments showed that the blank aggregates formed by the samples L-CS-DEAE$_{40}$D$_{5}$ and L-CS-DEAE$_{40}$D$_{28}$ had average sizes of 169 and 263 nm, respectively, and increased to 410 and 405 nm when loaded with quercetin. The zeta potential suggests that the surface of the nanoaggregates were positively charged and stable at physiological-like environment.

Drug safety assessment studies, including cell viability and hemolysis test, showed that the nanoaggregates were safe and very efficient at enhancing the effect of the quercetin in the control of the viability of breast cancer cells. Thus, the amphiphilic samples are important candidates for drug delivering systems.


AYDIN, R. S. T.; PULAT, M. 5-Fluorouracil Encapsulated Chitosan Nanoparticles for pH-Stimulated Drug Delivery: Evaluation of Controlled Release Kinetics. **Journal of Nanomaterials**, 2012.

CHOU, C. C.; YANG, J. S.; LU, H. F.; IP, S. W.; LO, C.; WU, C. C.; LIN, J. P.; TANG, N. Y.; CHUNG, J. G.; CHOU, M. J.; TENG, Y. H.; CHEN, D. R. Quercetin-mediated Cell Cycle Arrest and Apoptosis Involving Activation of a Caspase Cascade through the Mitochondria! Pathway in Human Breast Cancer MCF-7 Cells. **Archives of Pharmacal Research,** v. 33, n. 8, p. 1181-1191, Aug 2010.

COSTA, P.; MANUEL, J.; LOBO, S. Modeling and comparison of dissolution profiles. **European Journal of Pharmaceutical Sciences,** v. 13, n. 2, p. 123-133, May 2001.

DE OLIVEIRA PEDRO, R.; SCHMITT, C. C.; NEUMANN, M. G. Syntheses and characterization of amphiphilic quaternary ammonium chitosan derivatives. **Carbohydr Polym,** v. 147, p. 97-103, Aug 20 2016.

DE OLIVEIRA PEDRO, R.; TAKAKI, M.; GORAYEB, T. C.; DEL BIANCHI, V. L.; THOMEO, J. C.; TIERA, M. J.; DE OLIVEIRA TIERA, V. A. Synthesis, characterization and antifungal activity of quaternary derivatives of chitosan on Aspergillus flavus. **Microbiol Res,** v. 168, n. 1, p. 50-5, Jan 15 2013.

DU, H. L.; LIU, M. R.; YANG, X. Y.; ZHAI, G. X. The role of glycyrrhetinic acid modification on preparation and evaluation of quercetin-loaded chitosan-based self-aggregates. **Journal of Colloid and Interface Science,** v. 460, p. 87-96, Dec 15 2015.

HUANG, X.; BRAZEL, C. S. On the importance and mechanisms of burst release in matrix-controlled drug delivery systems. **Journal of Controlled Release,** v. 73, n. 2-3, p. 121-136, Jun 15 2001.

KORSMEYER, R. W.; GURNY, R.; DOELKER, E.; BURI, P.; PEPPAS, N. A. Mechanisms of Solute Release from Porous Hydrophilic Polymers. **International Journal of Pharmaceutics,** v. 15, n. 1, p. 25-35, 1983.

LAROCCA, L. M.; PIANTELLI, M.; LEONE, G.; SICA, S.; TEOFILI, L.; PANICI, P. B.; SCAMBIA, G.; MANCUSO, S.; CAPELLI, A.; RANELLETTI, F. O. Type-Ii Estrogen Binding-Sites in Acute Lymphoid and Myeloid Leukemias - Growth Inhibitory Effect of Estrogen and Flavonoids. **British Journal of Haematology,** v. 75, n. 4, p. 489-495, Aug 1990.

MITRA, T.; SAILAKSHMI, G.; GNANAMANI, A.; MANDAL, A. B. Studies on Cross-linking of Succinic Acid with Chitosan/Collagen. **Materials Research-Ibero-American Journal of Materials,** v. 16, n. 4, p. 755-765, Jul-Aug 2013.

PARK, J. K.; CHUNG, M. J.; CHOI, H. N.; PARK, Y. I. Effects of the Molecular Weight and the Degree of Deacetylation of Chitosan Oligosaccharides on Antitumor Activity. **International Journal of Molecular Sciences,** v. 12, n. 1, p. 266-277, Jan 2011.

PRALHAD, T.; RAJENDRAKUMAR, K. Study of freeze-dried quercetin-cyclodextrin binary systems by DSC, FT-IR, X-ray diffraction and SEM analysis. **Journal of Pharmaceutical and Biomedical Analysis,** v. 34, n. 2, p. 333-339, Feb 4 2004.

RINAUDO, M. Chitin and chitosan: Properties and applications. **Progress in Polymer Science,** v. 31, n. 7, p. 603-632, Jul 2006.

RINAUDO, M.; MILAS, M.; LEDUNG, P. Characterization of Chitosan - Influence of Ionic-Strength and Degree of Acetylation on Chain Expansion. **International Journal of Biological Macromolecules,** v. 15, n. 5, p. 281-285, Oct 1993.

RITGER, P. L.; PEPPAS, N. A. A simple equation for description of solute release I. Fickian and non-fickian release from non-swellable devices in the form of slabs, spheres, cylinders or discs. **Journal of Controlled Release,** v. 5, n. 1, p. 23-36, 1987/06/01 1987.

ROBLES, E.; JUAREZ, J.; BURBOA, M. G.; GUTIERREZ, L. E.; TABOADA, P.; MOSQUERA, V.; VALDEZ, M. A. Properties of Insulin- Chitosan Complexes Obtained by an Alkylation Reaction on Chitosan. **Journal of Applied Polymer Science,** v. 131, n. 6, Mar 15 2014.

STUART, M. A. C.; HUCK, W. T. S.; GENZER, J.; MULLER, M.; OBER, C.; STAMM, M.; SUKHORUKOV, G. B.; SZLEIFER, I.; TSUKRUK, V. V.; URBAN, M.; WINNIK, F.; ZAUSCHER, S.; LUZINOV, I.; MINKO, S. Emerging applications of stimuli-responsive polymer materials. **Nature Materials,** v. 9, n. 2, p. 101-113, Feb 2010.

TANNOCK, I. F.; ROTIN, D. Acid pH in tumors and its potential for therapeutic exploitation. **Cancer Res,** v. 49, n. 16, p. 4373-84, Aug 15 1989.

TOMMERAAS, K.; VARUM, K. M.; CHRISTENSEN, B. E.; SMIDSROD, O. Preparation and characterisation of oligosaccharides produced by nitrous acid depolymerisation of chitosans. **Carbohydrate Research,** v. 333, n. 2, p. 137-144, Jul 3 2001.

WU, M. M.; CAO, Z. Y.; ZHAO, Y. F.; ZENG, R.; TU, M.; ZHAO, J. H. Novel self-assembled pH-responsive biomimetic nanocarriers for drug delivery. **Materials Science & Engineering C-Materials for Biological Applications,** v. 64, p. 346-353, Jul 1 2016.

WU, M. M.; GUO, K.; DONG, H. W.; ZENG, R.; TU, M.; ZHAO, J. H. In vitro drug release and biological evaluation of biomimetic polymeric micelles self-assembled from amphiphilic deoxycholic acid-phospholylcholine-chitosan conjugate. **Materials Science & Engineering C-Materials for Biological Applications,** v. 45, p. 162-169, Dec 1 2014.

BRIGGER, I.; DUBERNET, C.; COUVREUR, P. Nanoparticles in cancer therapy and diagnosis. **Advanced Drug Delivery Reviews,** v. 54, n. 5, p. 631-651, Sep 13 2002.

DAMAGHI, M.; WOJTKOWIAK, J. W.; GILLIES, R. J. pH sensing and regulation in cancer. **Frontiers in Physiology,** v. 4, 2013.

HONARY, S.; ZAHIR, F. Effect of Zeta Potential on the Properties of Nano-Drug Delivery Systems - A Review (Part 2). **Tropical Journal of Pharmaceutical Research,** v. 12, n. 2, p. 265-273, Apr 2013.

KEAN, T.; THANOU, M. Biodegradation, biodistribution and toxicity of chitosan. **Advanced Drug Delivery Reviews,** v. 62, n. 1, p. 3-11, Jan 31 2010.

KUMAR, M. N. V. R. A review of chitin and chitosan applications. **Reactive & Functional Polymers,** v. 46, n. 1, p. 1-27, Nov 2000.

LI, X. Y.; KONG, X. Y.; ZHANG, Z. L.; NAN, K. H.; LI, L. L.; WANG, X. H.; CHEN, H. Cytotoxicity and biocompatibility evaluation of N,O-carboxymethyl chitosan/oxidized alginate hydrogel for drug delivery application. **International Journal of Biological Macromolecules,** v. 50, n. 5, p. 1299-1305, Jun 1 2012.

MERCHANT, Z.; TAYLOR, K. M. G.; STAPLETON, P.; RAZAK, S. A.; KUNDA, N.; ALFAGIH, I.; SHEIKH, K.; SALEEM, I. Y.; SOMAVARAPU, S. Engineering hydrophobically modified chitosan for enhancing the dispersion of respirable microparticles of levofloxacin. **European Journal of Pharmaceutics and Biopharmaceutics,** v. 88, n. 3, p. 816-829, Nov 2014.

NEL, A.; XIA, T.; MADLER, L.; LI, N. Toxic potential of materials at the nanolevel. **Science,** v. 311, n. 5761, p. 622-627, Feb 3 2006.

PEREZ-HERRERO, E.; FERNANDEZ-MEDARDE, A. Advanced targeted therapies in cancer: Drug nanocarriers, the future of chemotherapy. **European Journal of Pharmaceutics and Biopharmaceutics,** v. 93, p. 52-79, Jun 2015.

RAO, S. B.; SHARMA, C. P. Use of chitosan as a biomaterial: Studies on its safety and hemostatic potential. **Journal of Biomedical Materials Research,** v. 34, n. 1, p. 21-28, Jan 1997.

VAUPEL, P.; KALLINOWSKI, F.; OKUNIEFF, P. Blood-Flow, Oxygen and Nutrient Supply, and Metabolic Microenvironment of Human-Tumors - a Review. **Cancer Research,** v. 49, n. 23, p. 6449-6465, Dec 1 1989.

WANG, J. J.; ZENG, Z. W.; XIAO, R. Z.; XIE, T. A.; ZHOU, G. L.; ZHAN, X. R.; WANG, S. L. Recent advances of chitosan nanoparticles as drug carriers. **International Journal of Nanomedicine,** v. 6, p. 765-774, 2011.

ZHANG, C.; QU, G. W.; SUN, Y. J.; WU, X. J.; YAO, Z. L.; GUO, Q. L.; DING, Q. O.; YUAN, S. T.; SHEN, Z. L.; PING, Q. E.; ZHOU, H. P. Pharmacokinetics, biodistribution, efficacy and safety of N-octyl-O-sulfate chitosan micelles loaded with paclitaxel. **Biomaterials,** v. 29, n. 9, p. 1233-1241, Mar 2008.